Learning Disentangled Representations via Mutual Information Estimation

Eduardo H. Sanchez
IRT Saint Exupéry, IRIT
Toulouse, France

Mathieu Serrurier
IRIT
Toulouse, France

Mathias Ortner
IRT Saint Exupéry
Toulouse, France

Abstract

In this paper, we investigate the problem of learning disentangled representations. Given a pair of images sharing some attributes, we aim to create a low-dimensional representation which is split into two parts: a shared representation that captures the common information between the images and an exclusive representation that contains the specific information of each image. To address this issue, we propose a model based on mutual information estimation without relying on image reconstruction or image generation. Mutual information maximization is performed to capture the attributes of data in the shared and exclusive representations while we minimize the mutual information between the shared and exclusive representation to enforce representation disentanglement. We show that these representations are useful to perform downstream tasks such as image classification and image retrieval based on the shared or exclusive component. Moreover, classification results show that our model outperforms the state-of-the-art model based on VAE/GAN approaches in representation disentanglement.

1. Introduction

Deep learning success involves supervised learning where massive amounts of labeled data are used to learn useful representations from raw data. As labeled data is not always accessible, unsupervised learning algorithms have been proposed to learn useful data representations easily transferable for downstream tasks. A desirable property of these algorithms is to perform dimensionality reduction while keeping the most important attributes of data. For instance, methods based on deep neural networks have been proposed using autoencoder approaches [13, 16, 17] or generative models [1, 6, 10, 18, 20, 25]. Nevertheless, learning high-dimensional data can be challenging. Autoencoders present some difficulties to deal with multimodal data distributions and generative models rely on computationally demanding models [9, 15, 24] which are particularly complicated to train.

Recent work has focused on mutual information estimation and maximization to perform representation learning [2, 14, 22, 23]. As mutual information maximization is shown to be effective to capture the salient attributes of data, another desirable property is to be able to disentangle these attributes. For instance, it could be useful to remove some attributes of data that are not relevant for a given task such as illumination conditions in object recognition.

In particular, we are interested in learning representations of data that shares some attributes. Learning a representation that separates the common data attributes from the remaining data attributes could be useful in multiple situations. For example, capturing the common information from multiple face images could be advantageous to perform pose-invariant face recognition [27]. Similarly, learning a representation containing the common information across satellite image time series is shown to be useful for image classification and segmentation [26].

In this paper, we propose a method to learn disentangled representations based on mutual information estimation. Given an image pair (typically from different domains), we aim to disentangle the representation of these images into two parts: a shared representation that captures the common information between images and an exclusive representation that contains the specific information of each image. An example is shown in Figure 1. To capture the common information, we propose a novel method called *cross mutual information estimation and maximization*. Additionally, we propose an adversarial objective to minimize the mutual information between the shared and exclusive representations in order to achieve representation disentanglement. The following contributions are made in this work:

- Based on mutual information estimation (see Section 3), we propose a method to learn disentangled representations without relying on more costly image reconstruction or image generation models.

- In Section 4, we present a novel training procedure which is divided into two stages. First, the shared representation is learned via *cross mutual information estimation and maximization*. Secondly, mutual infor-
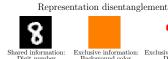
Figure 1: Representation disentanglement example. Given images X and Y on the left, our model aims to learn a representation space where the image information is split into the shared information (digit number) and the exclusive information (background/digit color) on the right.

mation maximization is performed to learn the exclusive representation while minimizing the mutual information between the shared and exclusive representations. We introduce an adversarial objective to minimize the mutual information as the method based on statistics networks described in Section 3 is not suitable for this purpose.

- In Section 5, we perform several experiments on two synthetic datasets: a) colored-MNIST [19]; b) 3D Shapes [4] and two real dataset: c) IAM Handwriting [21]; d) Sentinel-2 [7]. We show that the obtained representations are useful at image classification and image retrieval outperforming the state-of-the-art model based on VAE/GAN approaches in representation disentanglement. We perform an ablation study to analyze some components of our model. We also show the effectiveness of the proposed adversarial objective in representation disentanglement via a sensitivity analysis. In Section 6, we show the conclusions of our work.

2. Related work

Generative adversarial networks (GANs) The GAN model [10, 11] can be thought of as an adversarial game between two players: the generator and the discriminator. In this setting, the generator aims to produce samples that look like drawn from the data distribution $\mathbb{P}_{data}$ while the discriminator receives samples from the generator and the dataset to determine their source (dataset samples from $\mathbb{P}_{data}$ or generated samples from $\mathbb{P}_{gen}$). The generator is trained to fool the discriminator by learning a distribution $\mathbb{P}_{gen}$ that converges to $\mathbb{P}_{data}$.

Mutual information Recent work has focused on mutual information estimation and maximization as a means to perform representation learning. Since the mutual information is notoriously hard to compute for high-dimensional variables, some estimators based on deep neural networks have been proposed. Belghazi *et al.* [2] propose a mutual information estimator which is based on the Donsker-Varadhan representation of the Kullback-Leibler divergence. Instead,

Hjelm *et al.* [14] propose an objective function based on the Jensen-Shannon divergence called Deep InfoMax. Similarly, Ozair *et al.* [23] use the Wasserstein divergence. Mutual information maximization based methods learn representations without training decoder functions that go back into the image domain which is the prevalent paradigm in representation learning.

Representation disentanglement Disentangling data attributes can be useful for several tasks that require knowledge of these attributes. Creating representations where each dimension is independent and corresponds to a particular attribute have been proposed using VAE variants [13, 16]. Chen *et al.* [5] propose a GAN model combined with a mutual information regularization. Similar to our work, Gonzalez-Garcia *et al.* [9] propose a model based on VAE-GAN image translators and gradient reversal layers [8] to disentangle the attributes of paired data into shared and exclusive representations.

In this work, we aim to learn disentangled representations of paired data by splitting the representation into a shared part and an exclusive part. We propose a model based on mutual information estimation to perform representation learning using the method of Hjelm *et al.* [14] instead of generative or autoencoding models. Additionally, we introduce an adversarial objective [10] to disentangle the information contained in the shared and exclusive representations which is more effective than the gradient reversal layers [8]. We compare our model to the model proposed by Gonzalez-Garcia *et al.* [9] since we have a common goal: to disentangle the representation space into a shared and an exclusive representation for paired data. We show that we achieve better results for representation disentanglement.

3. Mutual information

Let $X \in \mathcal{X}$ and $Z \in \mathcal{Z}$ be two random variables. Assuming that $p(x, z)$ is the joint probability density function of X and Z and that $p(x)$ and $p(z)$ are the corresponding marginal probability density functions, the mutual information between X and Z can be expressed as follows

$$I(X, Z) = \int_{\mathcal{X}} \int_{\mathcal{Z}} p(x, z) \log \left(\frac{p(x, z)}{p(x)p(z)} \right) dx dz \quad (1)$$

From Equation 1, it can be seen that the mutual information $I(X, Z)$ can be written as the Kullback-Leibler divergence between the joint probability distribution $\mathbb{P}_{XZ}$ and the product of the marginal distributions $\mathbb{P}_X \mathbb{P}_Z$, *i.e.* $I(X, Z) = \mathrm{D}_{KL}\left(\mathbb{P}_{XZ} \parallel \mathbb{P}_X \mathbb{P}_Z \right)$.

In this work, we use the mutual information estimator Deep InfoMax [14] where the objective function is based on the Jensen-Shannon divergence instead, *i.e.* $I^{(\mathrm{JSD})}(X, Z) =$

$D_{JS}(\mathbb{P}_{XZ} \parallel \mathbb{P}_X \mathbb{P}_Z)$. We employ this method since it proves to be stable and we are not interested in the precise value of mutual information but in maximizing it. The estimator is shown in Equation 2 where $T_\theta : \mathcal{X} \times \mathcal{Z} \to \mathbb{R}$ is a deep neural network of parameters θ called the *statistics network*.

$$
\begin{aligned}
\hat{I}_\theta^{(\mathrm{JSD})}(X, Z) = \; & \mathbb{E}_{p(x,z)} \left[-\log\left(1 + e^{-T_\theta(x,z)}\right) \right] \\
& - \mathbb{E}_{p(x)p(z)} \left[\log\left(1 + e^{T_\theta(x,z)}\right) \right]
\end{aligned}
\quad (2)
$$

Hjelm *et al.* [14] propose an objective function based on the estimation and maximization of the mutual information between an image $X \in \mathcal{X}$ and its feature representation $Z \in \mathcal{Z}$ which is called *global mutual information*. The feature representation Z is extracted by a deep neural network of parameters ψ, $E_\psi : \mathcal{X} \to \mathcal{Z}$. Equation 3 displays the global mutual information objective.

$$
\mathbf{L}_{\theta,\psi}^{\mathrm{global}}(X, Z) = \hat{I}_\theta^{(\mathrm{JSD})}(X, Z) \quad (3)
$$

Additionally, Hjelm *et al.* [14] propose to maximize the mutual information between local patches of the image X represented by a feature map $C_\psi(X)$ of the encoder $E_\psi = f_\psi \circ C_\psi$ and the feature representation Z which is called *local mutual information*. Equation 4 shows the local mutual information objective.

$$
\mathbf{L}_{\phi,\psi}^{\mathrm{local}}(X, Z) = \hat{I}_\phi^{(\mathrm{JSD})}(C_\psi(X), Z) \quad (4)
$$

4. Method

Let X and Y be two images belonging to the domains $\mathcal{X}$ and $\mathcal{Y}$ respectively. Let $R_X \in \mathcal{R}_\mathcal{X}$ and $R_Y \in \mathcal{R}_\mathcal{Y}$ be the corresponding representations for each image. The representation is split into two parts: the shared representations S_X and S_Y which contain the common information between the images X and Y and the exclusive representations E_X and E_Y which contain the specific information of each image. Therefore the representation of image X can be written as $R_X = (S_X, E_X)$. Similarly, we can write $R_Y = (S_Y, E_Y)$ for image Y. For instance, let us consider the images shown in Figure 1. In this case, the shared representations S_X and S_Y contain the digit number information while the exclusive representations E_X and E_Y correspond to the background and digit color information.

To address this representation disentanglement, we propose a training procedure which is split into two stages. We think that a natural way to learn these disentangled representations can be done via an incremental approach. The first stage learns the common information between images and creates a shared representation (see Section 4.1). Knowing the common information, it is easy then to identify the specific information of each image. Therefore, us-

ing the shared representation from the previous stage, a second stage is then performed to learn the exclusive representation (see Section 4.2) which captures the remaining information that is missing in the shared representation. The model overview can be seen in Figure 2.

4.1. Shared representation learning

Let $E_{\psi_X}^{\mathrm{sh}} : \mathcal{X} \to \mathcal{S}_\mathcal{X}$ and $E_{\psi_Y}^{\mathrm{sh}} : \mathcal{Y} \to \mathcal{S}_\mathcal{Y}$ be the encoder functions to extract the shared representations S_X and S_Y from images X and Y, respectively. We estimate and maximize the mutual information between the images and their shared representations via Equations 3 and 4 using the global statistics networks $T_{\theta_X}^{\mathrm{sh}}$ and $T_{\theta_Y}^{\mathrm{sh}}$ and the local statistics networks $T_{\phi_X}^{\mathrm{sh}}$ and $T_{\phi_Y}^{\mathrm{sh}}$. In contrast to Deep Info-Max [14], to enforce to learn only the common information between images X and Y, we switch the shared representations to compute the *cross mutual information* as shown in Equation 5 where global and local mutual information terms are weighted by constant coefficients α^{sh} and β^{sh}. Switching the shared representations is a key element of the proposed method as it enforces to remove the exclusive information of each image (see Section 5.3).

$$
\begin{aligned}
\mathbf{L}_{MI}^{\mathrm{sh}} = \; & \alpha^{\mathrm{sh}}(\mathbf{L}_{\theta_X,\psi_Y}^{\mathrm{global}}(X, S_Y) + \mathbf{L}_{\theta_Y,\psi_X}^{\mathrm{global}}(Y, S_X)) \\
& + \beta^{\mathrm{sh}}\left(\mathbf{L}_{\phi_X,\psi_Y}^{\mathrm{local}}(X, S_Y) + \mathbf{L}_{\phi_Y,\psi_X}^{\mathrm{local}}(Y, S_X)\right)
\end{aligned}
\quad (5)
$$

Additionally, images X and Y must have identical shared representations, *i.e.* $S_X = S_Y$. A simple solution is to minimize the L_1 distance between their shared representations as follows

$$
\mathbf{L}_1 = \mathbb{E}_{p(s_x,s_y)}\left[|S_X - S_Y|\right] \quad (6)
$$

The objective function to learn the shared representations is a linear combination of the previous loss terms as can be seen in Equation 7, where γ is a constant coefficient.

$$
\max_{\{\psi,\theta,\phi\}_{X,Y}} \mathcal{L}^{\mathrm{shared}} = \mathbf{L}_{MI}^{\mathrm{sh}} - \gamma \mathbf{L}_1 \quad (7)
$$

4.2. Exclusive representation learning

So far, our model is able to extract the shared representations S_X and S_Y. Let $E_{\omega_X}^{\mathrm{ex}} : \mathcal{X} \to \mathcal{E}_\mathcal{X}$ and $E_{\omega_Y}^{\mathrm{ex}} : \mathcal{Y} \to \mathcal{E}_\mathcal{Y}$ be the encoder functions to extract the exclusive representations E_X and E_Y from images X and Y, respectively. To learn these representations, we estimate and maximize the mutual information between the image X and its corresponding representation R_X which is composed of the shared and exclusive representations *i.e.* $R_X = (S_X, E_X)$. The same operation is performed between the image Y and $R_Y = (S_Y, E_Y)$ as shown in Equation 8 where α^{ex} and β^{ex} are constant coefficients. Mutual information is computed by the global statistics networks $T_{\theta_X}^{\mathrm{ex}}$ and $T_{\theta_Y}^{\mathrm{ex}}$ and the local statistics networks $T_{\phi_X}^{\mathrm{ex}}$ and $T_{\phi_Y}^{\mathrm{ex}}$. Since the shared representation remains constant, we enforce the exclusive representation to include the information which is specific to the
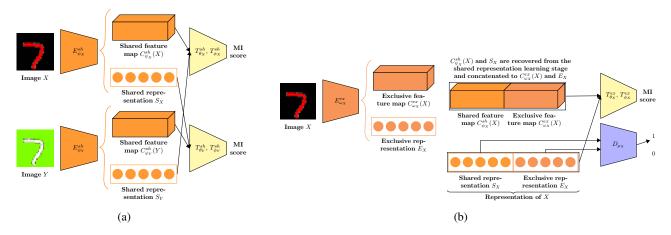
Figure 2: Model overview. a) First, the shared representation is learned. Images X and Y are passed through the shared representation encoders to extract the representations S_X and S_Y. The statistics networks maximize the mutual information between the image X and the representation S_Y (and between Y and S_X); b) Then, the exclusive representation is learned. The image X is passed through the exclusive representation encoder to obtain the representation E_X. The statistics networks maximize the mutual information between the image X and its representation $R_X = (S_X, E_X)$ while the discriminator minimize the mutual information between representations S_X and E_X. The same operation is performed to learn E_Y.

image and is not captured by the shared representation.

$$\mathbf{L}_{MI}^{\mathrm{ex}} = \alpha^{\mathrm{ex}}(\mathbf{L}_{\theta_X,\omega_X}^{\mathrm{global}}(X, R_X) + \mathbf{L}_{\theta_Y,\omega_Y}^{\mathrm{global}}(Y, R_Y)) \\ + \beta^{\mathrm{ex}}\left(\mathbf{L}_{\phi_X,\omega_X}^{\mathrm{local}}(X, R_X) + \mathbf{L}_{\phi_Y,\omega_Y}^{\mathrm{local}}(Y, R_Y)\right) \quad (8)$$

On the other hand, the representation E_X must not contain information captured by the representation S_X when maximizing the mutual information between X and R_X. Therefore, the mutual information between E_X and S_X must be minimized. While mutual information estimation and maximization via Equation 2 works well, using statistics networks fails to converge when performing mutual information estimation and minimization. Therefore, we propose to minimize the mutual information between S_X and E_X via a different implementation of Equation 2 using an adversarial objective [10] as shown in Equation 9. A discriminator D_{ρ_X} defined by a neural network of parameters ρ_X is trained to classify representations drawn from $\mathbb{P}_{S_X E_X}$ as fake samples and representations drawn from $\mathbb{P}_{S_X}\mathbb{P}_{E_X}$ as real samples. Samples from $\mathbb{P}_{S_X E_X}$ are obtained by passing the image X through the encoders $E_{\psi_X}^{\mathrm{sh}}$ and $E_{\omega_X}^{\mathrm{ex}}$ to extract (S_X, E_X). Samples from $\mathbb{P}_{S_X}\mathbb{P}_{E_X}$ are obtained by shuffling the exclusive representations of a batch of samples from $\mathbb{P}_{S_X E_X}$. The encoder function $E_{\omega_X}^{\mathrm{ex}}$ strives to generate exclusive representations E_X that combined with S_X look like drawn from $\mathbb{P}_{S_X}\mathbb{P}_{E_X}$. By minimizing Equation 9, we minimize the Jensen-Shannon divergence $\mathrm{D}_{JS}\left(\mathbb{P}_{S_X E_X} \parallel \mathbb{P}_{S_X}\mathbb{P}_{E_X}\right)$ and thus the mutual information between E_X and S_X is minimized. A similar procedure to generate samples of the product of the marginal distributions from samples of the joint probability distribution is proposed in [3, 16]. In these models, an adversarial objective is used to make each di-

mension independent of the remaining dimensions of the representation. Instead, we use an adversarial objective to make the dimensions of the shared part independent of the dimensions of the exclusive part.

$$\mathbf{L}_{\mathrm{adv}}^X = \mathbb{E}_{p(s_x)p(e_x)}\left[\log D_{\rho_X}(S_X, E_X)\right] \\ + \mathbb{E}_{p(s_x,e_x)}\left[\log\left(1 - D_{\rho_X}(S_X, E_X)\right)\right] \quad (9)$$

Equation 10 shows the objective function to learn the exclusive representation which is a linear combination of the previous loss terms where λ_{adv} is a constant coefficient.

$$\max_{\{\omega,\theta,\phi\}_{X,Y}} \min_{\{\rho\}_{X,Y}} \mathcal{L}^{\mathrm{ex}} = \mathbf{L}_{MI}^{\mathrm{ex}} - \lambda_{\mathrm{adv}}(\mathbf{L}_{\mathrm{adv}}^X + \mathbf{L}_{\mathrm{adv}}^Y) \quad (10)$$

4.3. Implementation details

Concerning the model architecture, we use DCGAN-like encoders [25], statistics networks similar to those used in Deep InfoMax [14] and a discriminator defined by a fully-connected network with 3 layers. Every network is trained from scratch using batches of 64 image pairs. We use Adam optimizer with a learning rate value of 0.0001. Concerning the loss coefficients, we use $\alpha^{\mathrm{sh}} = \alpha^{\mathrm{ex}} = 0.5$, $\beta^{\mathrm{sh}} = \beta^{\mathrm{ex}} = 1.0$, $\gamma = 0.1$. The coefficient λ_{adv} is analyzed in Section 5.3. The training algorithm is executed on a NVIDIA Tesla P100. More details about the architecture, hyperparameters and optimizer are provided in the supplementary material section. We also provide our code to train the model and run the experiments.
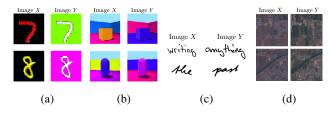
Figure 3: Image pair samples (best viewed in color). (a) Colored-MNIST; (b) 3D Shapes; (c) IAM; (d) Sentinel-2.

5. Experiments

5.1. Datasets

We perform representation disentanglement on the following datasets: a) **Colored-MNIST**: Similarly to Gonzalez-Garcia [9], we use a colored version of the MNIST dataset [19]. The colored background MNIST dataset (MNIST-CB) is generated by modifying the color of the background and the colored digit MNIST dataset (MNIST-CD) is generated by modifying the digit color. The background/digit color is randomly selected from a set of 12 colors. Two images with the same digit are sampled from MNIST-CB and MNIST-CD to create an image pair; b) **3D Shapes**: The 3D Shapes dataset [4] is composed of 480000 images of $64{\times}64{\times}3$ pixels. Each image corresponds to a 3D object in a room with six factors of variation: floor color, wall color, object color, object scale, object shape and scene orientation. These factors of variation have 10, 10, 10, 8, 4 and 15 possible values respectively. We create a new dataset which consists of image pairs where the object scale, object shape and scene orientation are the same for both images while the floor color, wall color and object color are randomly selected; c) **IAM**: The IAM dataset [21] is composed of forms of handwritten English text. Words contained in the forms are isolated and labeled which can be used to train models to perform handwritten text recognition or writer identification. To train our model we select a subset of 6711 images of $64{\times}256{\times}1$ pixels corresponding to the top 50 writers. Our dataset is composed of image pairs where both images correspond to words written by the same person; d) **Sentinel-2**: Similarly to [26], we create a dataset composed of optical images of size $64{\times}64$ from the Sentinel-2 mission [7]. A 100GB dataset is created by selecting several regions of interest on the Earth's surface. Image pairs are created by selecting images from the same region but acquired at different times. Further details about the dataset creation can be found on the supplementary material. Some dataset image examples are shown in Figure 3. For all the datasets, we train our model to learn a shared representation of size 64. An exclusive representation of size 8, 64 and 64 is respectively learned for the colored-MNIST, 3D Shapes and IAM datasets. During

training, when data comes from a single domain the number of networks involved can be halved by sharing weights (*i.e.* $\psi_X{=}\psi_Y$, $\theta_X{=}\theta_Y$, etc). For example, the reported results for the 3D Shapes, Sentinel-2 and IAM datasets are obtained using 3 networks (shared representation encoder, global and local statistics networks) to learn the shared representation and 4 networks (discriminator, exclusive representation encoder, global and local statistics networks) to learn the exclusive representation.

5.2. Representation disentanglement evaluation

To evaluate the learned representations, we perform several classification experiments. A classifier trained on the shared representation should be good for classifying the shared attributes of the image as the shared representation only contains the common information while it should achieve a performance close to random for classifying the exclusive attributes of the image. An analogous case occurs when performing classification using the exclusive representation. We use a simple architecture composed of 2 hidden fully-connected layers of few neurons to implement the classifier (more details in the supplementary material).

In the colored-MNIST dataset case, a classifier trained on the shared representation must perform well at digit number classification while the accuracy must be close to 8.33% (random decision between 12 colors) at background/digit color classification since no exclusive information is included in the shared representation. Similarly, using the exclusive representations to train a classifier, we expect the classifier to predict correctly the background/digit color while achieving a digit number accuracy close to 10% (random decision between 10 digits) as the exclusive representations contains no digit number information. Results are shown in Tables 1 and 2. We note that the learned representations by our model achieve the expected behavior. The same experiment is performed using the learned representations from the 3D Shapes dataset. A classifier trained on the shared representation must correctly classify the object scale, object shape and scene orientation while the accuracy must be close to random for the floor, wall and object colors (10%, random decision between 10 colors). Differently, a classifier trained on the exclusive representation must correctly classify the floor, wall and object colors while it must achieve a performance close to random to classify the object scale (12.50%, random decision between 8 scales), object shape (25%, random decision between 4 shapes) and scene orientation (6.66%, random decision between 15 orientations). Accuracy results using the shared and exclusive representations are shown in Table 3.

For the colored-MNIST and 3D Shapes datasets, we compare our representations to the representations obtained from the model proposed by Gonzalez-Garcia *et al.* [9] using their code. In their model, even if the exclusive fac-

Method	Background color	Digit number	Distance to ideal
Ideal feature S_X	8.33%	100.00%	0.0000
Feature S_X (ours)	**8.22%**	**94.48%**	**0.0563**
Feature S_X ([9])	99.56%	95.42%	0.9581
Ideal feature E_X	100.00%	10.00%	0.0000
Feature E_X (ours)	**99.99%**	**13.20%**	**0.0321**
Feature E_X ([9])	99.99%	71.63%	0.6164

Table 1: Background color and digit number accuracy using the shared representation S_X and the exclusive representation E_X.

Method	Digit color	Digit number	Distance to ideal
Ideal feature S_Y	8.33%	100.00%	0.0000
Feature S_Y (ours)	**8.83%**	**94.27%**	**0.0623**
Feature S_Y ([9])	29.81%	95.06%	0.2641
Ideal feature E_Y	100.00%	10.00%	0.0000
Feature E_Y (ours)	**99.92%**	**13.75%**	**0.0383**
Feature E_Y ([9])	99.83%	74.54%	0.6471

Table 2: Digit color and number accuracy using the shared representation S_Y and the exclusive representations E_Y.

Method	Floor color	Wall color	Object color	Object scale	Object shape	Scene Orientation	Distance to ideal
Ideal feature S_X	10.00%	10.00%	10.00%	100.00%	100.00%	100.00%	0.0000
Feature S_X (ours)	**9.96%**	**10.08%**	**9.95%**	**99.99%**	**99.99%**	**99.99%**	**0.0020**
Feature S_X ([9])	99.92%	99.81%	96.67%	99.99%	99.99%	99.99%	2.6643
Ideal feature E_X	100.00%	100.00%	100.00%	12.50%	25.00%	6.66%	0.0000
Feature E_X (ours)	**95.10%**	**99.79%**	**96.17%**	**17.25%**	**30.73%**	**6.79%**	**0.1955**
Feature E_X ([9])	99.99%	99.99%	99.94%	99.06%	99.98%	99.81%	2.5477

Table 3: Accuracy on the 3D Shapes factors using the disentangled representations S_X and E_X.

tors at image generation are controlled by the exclusive representation, the classification experiment shows that representation disentanglement is not correctly performed as the shared representation contains exclusive information and vice versa. In all the cases, the representations of our model are much closer in terms of accuracy to the ideal disentangled representations than the representations from the model of [9]. We compute the distance to the ideal representation as the L_1 distance between the accuracies on data attributes. As representations obtained from generative models are determined by an objective function defined in the image domain, disentanglement constraints are not explicitly defined in the representation domain. Therefore, representation disentanglement is deficiently achieved in generative models. Moreover, our model is less computationally demanding as it does not require decoder functions to go back into the image domain. Training our model on the colored-MNIST dataset takes 20 min/epoch while the model of [9] takes 115 min/epoch.

For the IAM dataset, as the shared representation must capture the writer style, it must be useful to perform writer recognition while the exclusive representation must be useful to perform word classification. Accuracy results based on these representations can be seen in Table 4. Reasonable results are obtained at writer recognition while less satisfactory results are obtained at word classification as it is a more difficult task. To provide a comparison, we use the latent representation of size 128 learned by a VAE model [17] (as the model of [9] fails to converge) to train a classifier

for the mentioned classification tasks. Table 4 shows that the shared representation outperforms the VAE representation for writer recognition and the exclusive representation achieves a similar performance for word classification.

Additionally, we perform image retrieval experiments using the learned representations. In the colored-MNIST dataset, using the shared representation of a query image retrieves images containing the same digit independently of the background/digit color. In contrast, using the exclusive representation of a query image retrieves images corresponding to the same background/digit color independently of the digit number. A similar case occurs for the 3D Shapes dataset. In the IAM dataset, using the shared representations retrieves words written by the same person or similar style. While using the exclusive representation seems to retrieve images corresponding to the same word. Some image retrieval examples using the shared and exclusive representations are shown in Figure 4. As image retrieval is useful for clustering attributes, we also perform writer and word recognition on the IAM dataset using $N \in \{1, 5\}$ nearest neighbors based on the disentangled representations. We achieve similar results to those obtained using a neural network classifier as shown in Table 5.

5.3. Analysis of the objective function

Ablation study To evaluate the contribution of each element of the model during the shared representation learning, we remove it and observe the impact on the classification accuracy on the data attributes. As described in Sec-

Method	Writer	Word
Ideal feature S_X	100.00%	$\sim 1.00\%$
Ideal feature E_X	$\sim 2.00\%$	100.00%
Feature S_X (ours)	**61.64%**	**9.94%**
Feature E_X (ours)	**10.80%**	**20.88%**
Feature f_X ([17])	13.77%	20.30%

Table 4: Writer and word recognition accuracy.

Method	Writer	Word
Feature S_X ($N=1$)	62.65%	15.78%
Feature S_X ($N=5$)	64.06%	12.96%
Feature E_X ($N=1$)	19.68%	19.84%
Feature E_X ($N=5$)	16.87%	19.69%

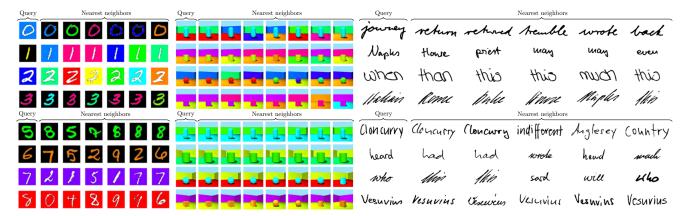Table 5: Writer and word recognition accuracy using N nearest neighbors.

Figure 4: Image retrieval on the colored-MNIST, 3D Shapes and IAM datasets (best viewed in color and zoom-in). Retrieved images using the shared representations (on the top) and the exclusive representations (on the bottom).

Method	Background color	Digit number	Distance to ideal
Ideal feature S_X	8.33%	100.00%	0.0000
Baseline	**8.22%**	**94.48%**	**0.0563**
Baseline (non-SSR)	99.99%	89.57%	1.0209
Baseline ($\gamma = 0$)	8.49%	92.36%	0.0780
Baseline ($\alpha^{\text{sh}} = 0$)	11.11%	94.83%	0.0795
Baseline ($\beta^{\text{sh}} = 0$)	8.51%	80.59%	0.1958

Table 6: MNIST ablation study. Accuracy using S_X.

Method	Word	Writer	Distance to ideal
Ideal feature S_X	$\sim 1.00\%$	100.00%	0.0000
Baseline	**9.94%**	**61.64%**	**0.4730**
Baseline (non-SSR)	20.88%	58.94%	0.6094
Baseline ($\gamma = 0$)	10.51%	55.39%	0.5412
Baseline ($\alpha^{\text{sh}} = 0$)	11.36%	61.50%	0.4886
Baseline ($\beta^{\text{sh}} = 0$)	13.63%	50.28%	0.6235

Table 7: IAM ablation study. Accuracy using S_X.
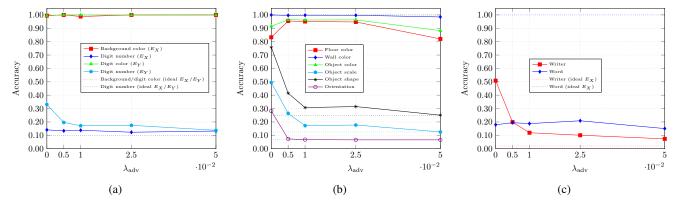

(a)

(b)

(c)

Figure 5: Different values of λ_{adv} are used to learn the exclusive representation. Results are plotted in terms of factor accuracy as a function of λ_{adv}. Solid curves correspond to the obtained values and dotted curves correspond to the expected behavior of an ideal exclusive representation (best viewed in color). (a) Colored-MNIST; (b) 3D Shapes; (c) IAM datasets.

tion 4.3, our baseline setting is the following: $\alpha^{\mathrm{sh}} = 0.5$, $\beta^{\mathrm{sh}} = 1.0$, $\gamma = 0.1$ and switched shared representations S_X/S_Y (SSR). We perform the ablation study and show the results for the colored-MNIST and IAM datasets in Tables 6 and 7. Switching the shared representations plays a crucial role in representation disentanglement avoiding these representations to capture exclusive information. When the shared representations are not switched (non-SSR), the accuracy on exclusive attributes considerably increases meaning the presence of exclusive information in the shared representations. Removing the L_1 distance between S_X and S_Y ($\gamma = 0$) slightly reduces the accuracy on shared attributes. Removing the global mutual information term ($\alpha^{\mathrm{sh}} = 0$) slightly increases the presence of exclusive information in the shared representation. Finally, using the local mutual information term is important to capture the shared information as the accuracy on shared attributes considerably decreases when setting $\beta^{\mathrm{sh}} = 0$. Similar results are obtained by setting $\alpha^{\mathrm{ex}} = 0$ or $\beta^{\mathrm{ex}} = 0$ during the exclusive representation learning. In general, all loss terms lead to an improvement in representation disentanglement.

Sensitivity analysis As the parameter λ_{adv} weights the term that minimizes the mutual information between the shared and exclusive representations, we empirically investigate the impact of this parameter on the information captured by the exclusive representation. We use different values of $\lambda_{\mathrm{adv}} \in \{0.0, 0.005, 0.010, 0.025, 0.05\}$ to train our model. Then, exclusive representations are used to perform classification on the attributes of data. Results in terms of accuracy as a function of λ_{adv} are shown in Figure 5. For $\lambda_{\mathrm{adv}} = 0.0$ no representation disentanglement is performed, then the exclusive representation contains shared information and achieves a classification performance higher than random for the shared attributes of data. While increasing the value of λ_{adv} the exclusive representation behavior (solid curves) converges to the expected behavior (dotted curves). However, values higher than 0.025 decrease the performance classification on exclusive attributes of data.

5.4. Satellite applications

We show that our model is particularly useful when large amounts of unlabeled data are available and labels are scarce as in the case of satellite data. We train our model to learn the shared representations of our Sentinel-2 dataset which contains 100GB of unlabeled data. Then, a classifier is trained on the EuroSAT dataset [12] (27000 Sentinel-2 images of size $64{\times}64$ labeled in 10 classes) using the learned representations of our model as inputs. While training a classifier on the shared representation, we make it robust to time-related conditions (seasonal changes, atmospheric conditions, etc.). We achieve an accuracy of 93.11%

outperforming the performance obtained using the representations of a VAE model [17] (87.64%) and the VAE-GAN model proposed by Sanchez *et al*. [26] (92.38%).

As another interesting application, we found that Equation 5 could be used to measure the distance between the center pixels of image patches X and Y in terms of mutual information. Some examples are shown in Figure 6. As can be seen, using this distance we are able to distinguish the river, urban regions and agricultural areas. We think this could be useful for further applications such as unsupervised image segmentation and object detection.
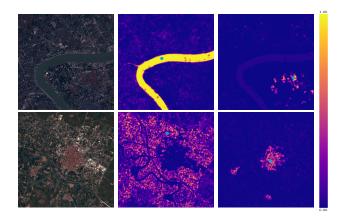

Figure 6: Pixel distance based on mutual information. The mutual information is computed between a given pixel (blue point) and the remaining image pixels via Equation 5.

6. Conclusions

We have proposed a novel method to perform representation disentanglement on paired images based on mutual information estimation using a two-stage training procedure. We have shown that our model is less computationally demanding and outperforms the VAE-GAN model of [9] to disentangle representations via classification experiments in three datasets. Additionally, we have performed an ablation study to demonstrated the usefulness of the key elements of our model (switched shared representations, local and global statistics networks) and their impact on representation disentanglement. Then, we have empirically proven the disentangling capability of our model by analyzing the role of λ_{adv} during training. Finally, we have demonstrated the benefits of our model on a challenging setting where large amounts of unlabeled paired data are available as in the Sentinel-2 case. We have shown that our model outperforms models relying on image reconstruction or image generation at image classification. We have also shown that the *cross mutual information* objective could be useful for unsupervised image segmentation and object detection.

References

[1] Martin Arjovsky, Soumith Chintala, and Léon Bottou. Wasserstein generative adversarial networks. In *Proceedings of the 34th International Conference on Machine Learning*, 2017. 1

[2] Mohamed Ishmael Belghazi, Aristide Baratin, Sai Rajeshwar, Sherjil Ozair, Yoshua Bengio, Aaron Courville, and Devon Hjelm. Mutual information neural estimation. In *Proceedings of the 35th International Conference on Machine Learning*, 2018. 1, 2

[3] Philemon Brakel and Yoshua Bengio. Learning independent features with adversarial nets for non-linear ica. *arXiv preprint arXiv:1710.05050*, 2017. 4

[4] Chris Burgess and Hyunjik Kim. 3d shapes dataset. https://github.com/deepmind/3dshapes-dataset/, 2018. 2, 5

[5] Xi Chen, Yan Duan, Rein Houthooft, John Schulman, Ilya Sutskever, and Pieter Abbeel. Infogan: Interpretable representation learning by information maximizing generative adversarial nets. In *Advances in Neural Information Processing Systems*, 2016. 2

[6] Jeff Donahue, Philipp Krähenbühl, and Trevor Darrell. Adversarial feature learning. In *International Conference on Learning Representations*, 2017. 1

[7] Matthias Drusch, Umberto Del Bello, Sébastien Carlier, Olivier Colin, Veronica Fernandez, Ferran Gascon, Bianca Hoersch, Claudia Isola, Paolo Laberinti, Philippe Martimort, et al. Sentinel-2: Esa's optical high-resolution mission for gmes operational services. *Remote sensing of Environment*, 120:25–36, 2012. 2, 5

[8] Yaroslav Ganin and Victor Lempitsky. Unsupervised domain adaptation by backpropagation. In *Proceedings of the 32nd International Conference on Machine Learning*, 2015. 2

[9] Abel Gonzalez-Garcia, Joost van de Weijer, and Yoshua Bengio. Image-to-image translation for cross-domain disentanglement. In *Advances in Neural Information Processing Systems*. 2018. 1, 2, 5, 6, 8

[10] Ian Goodfellow, Jean Pouget-Abadie, Mehdi Mirza, Bing Xu, David Warde-Farley, Sherjil Ozair, Aaron Courville, and Yoshua Bengio. Generative adversarial nets. In *Advances in neural information processing systems*, 2014. 1, 2, 4

[11] Ian J. Goodfellow. NIPS 2016 tutorial: Generative adversarial networks. 2016. 2

[12] Patrick Helber, Benjamin Bischke, Andreas Dengel, and Damian Borth. Eurosat: A novel dataset and deep learning benchmark for land use and land cover classification. *CoRR*, abs/1709.00029, 2017. 8

[13] Irina Higgins, Loic Matthey, Arka Pal, Christopher Burgess, Xavier Glorot, Matthew Botvinick, Shakir Mohamed, and Alexander Lerchner. beta-vae: Learning basic visual concepts with a constrained variational framework. In *International Conference on Learning Representations*, 2017. 1, 2

[14] R Devon Hjelm, Alex Fedorov, Samuel Lavoie-Marchildon, Karan Grewal, Phil Bachman, Adam Trischler, and Yoshua Bengio. Learning deep representations by mutual information estimation and maximization. In *International Conference on Learning Representations*, 2019. 1, 2, 3, 4

[15] Tero Karras, Samuli Laine, and Timo Aila. A style-based generator architecture for generative adversarial networks. In *Proceedings of the IEEE Conference on Computer Vision and Pattern Recognition*, 2019. 1

[16] Hyunjik Kim and Andriy Mnih. Disentangling by factorising. In *Proceedings of the 35th International Conference on Machine Learning*, 2018. 1, 2, 4

[17] Diederik P Kingma and Max Welling. Auto-encoding variational bayes. In *International Conference on Learning Representations*, 2014. 1, 6, 7, 8

[18] Anders Boesen Lindbo Larsen, Sren Kaae Snderby, Hugo Larochelle, and Ole Winther. Autoencoding beyond pixels using a learned similarity metric. In *Proceedings of The 33rd International Conference on Machine Learning*, 2016. 1

[19] Yann LeCun and Corinna Cortes. MNIST handwritten digit database. 2010. 2, 5

[20] Xudong Mao, Qing Li, Haoran Xie, Raymond YK Lau, Zhen Wang, and Stephen Paul Smolley. Least squares generative adversarial networks. In *2017 IEEE International Conference on Computer Vision (ICCV)*, 2017. 1

[21] U-V Marti and Horst Bunke. The IAM-database: an english sentence database for offline handwriting recognition. *International Journal on Document Analysis and Recognition*, 2002. 2, 5

[22] Aaron van den Oord, Yazhe Li, and Oriol Vinyals. Representation learning with contrastive predictive coding. *arXiv preprint arXiv:1807.03748*, 2018. 1

[23] Sherjil Ozair, Corey Lynch, Yoshua Bengio, Aaron van den Oord, Sergey Levine, and Pierre Sermanet. Wasserstein dependency measure for representation learning. *arXiv preprint arXiv:1903.11780*, 2019. 1, 2

[24] Taesung Park, Ming-Yu Liu, Ting-Chun Wang, and Jun-Yan Zhu. Semantic image synthesis with spatially-adaptive normalization. In *Proceedings of the IEEE Conference on Computer Vision and Pattern Recognition*, 2019. 1

[25] Alec Radford, Luke Metz, and Soumith Chintala. Unsupervised representation learning with deep convolutional generative adversarial networks. In *International Conference on Learning Representations*, 2016. 1, 4

[26] Eduardo Sanchez, Mathieu Serrurier, and Mathias Ortner. Learning disentangled representations of satellite image time series. In *Proceedings of the European Conference on Machine Learning and Principles and Practice of Knowledge Discovery in Databases*, 2019. 1, 5, 8

[27] Luan Tran, Xi Yin, and Xiaoming Liu. Disentangled representation learning gan for pose-invariant face recognition. In *Proceedings of the IEEE Conference on Computer Vision and Pattern Recognition*, 2017. 1